



HAL
open science

Green nanoceramic pigments based on cobalt chromite doped with Al: Synthesis, characterisation and colour performance

Youssef El Jabbar, Hind Lakhlifi, Rachida El Ouatib, Lahcen Er-Rakho,
Sophie Guillemet-Fritsch, Bernard Durand

► To cite this version:

Youssef El Jabbar, Hind Lakhlifi, Rachida El Ouatib, Lahcen Er-Rakho, Sophie Guillemet-Fritsch, et al.. Green nanoceramic pigments based on cobalt chromite doped with Al: Synthesis, characterisation and colour performance. *Ceramics International*, 2020, 47 (7, Part A), pp.9373 - 9381. 10.1016/j.ceramint.2020.12.068 . hal-03851445

HAL Id: hal-03851445

<https://hal.science/hal-03851445>

Submitted on 23 Nov 2022

HAL is a multi-disciplinary open access archive for the deposit and dissemination of scientific research documents, whether they are published or not. The documents may come from teaching and research institutions in France or abroad, or from public or private research centers.

L'archive ouverte pluridisciplinaire **HAL**, est destinée au dépôt et à la diffusion de documents scientifiques de niveau recherche, publiés ou non, émanant des établissements d'enseignement et de recherche français ou étrangers, des laboratoires publics ou privés.

Green nanoceramic pigments based on cobalt chromite doped with Al: synthesis, characterisation and colour performance

Youssef El Jabbar^{a,*}, Hind Lakhlifi^a, Rachida El Ouatib^a, Lahcen Er-Rakho^a, Sophie Guillemet-Fritsch^b, Bernard Durand^b

^a Laboratoire de Physico-chimie des Matériaux Inorganiques, Faculté des sciences Aïn chock, Université Hassan II, Bb. 5366 Mâarif, Casablanca, Morocco.

^b Institut Carnot CIRIMAT, CNRS Université de Toulouse, 118 route de Narbonne, 31062 Toulouse Cedex 9, France.

* Corresponding author email: ysf.eljabbar@gmail.com (youssef El Jabbar)

Abstract

Nano-sized spinel cobalt chromite oxide CoCr_2O_4 and its substituted forms $\text{CoCr}_{2-x}\text{Al}_x\text{O}_4$ ($0 \leq x \leq 2$) have been successfully synthesised by wet chemical route. The prepared powders were characterised by means of thermal analysis (DTA/TGA), X-ray diffraction (XRD), Field emission scanning electron microscopy (FE-SEM), Brunauer–Emmett–Teller analysis (BET), UV-visible techniques (UV-Vis) and colorimetric analyses (L^* a^* b^*). The results show that the $\text{CoCr}_{2-x}\text{Al}_x\text{O}_4$ ($0 \leq x \leq 2$) samples are in the crystalline phase at 900°C with a particle size range of 20–200 nm. The colouration of the synthesised pigments is sensitive to the distribution of doping trivalent ions in the spinel lattice. The Al-enrichment leads to a colour shift from green to blue and the grains become more and more spherical and less agglomerated. Green cobalt chromite powders were substituted with 50% aluminium (CoCrAlO_4), allowing the specific surface area of green nanometric powders to be increased from 7.4 to $12.4 \text{ m}^2/\text{g}$.

Keywords: Chromite spinel; Nanoparticles; Chemical route; Ceramics; Optical proprieties.

1. Introduction

In the ceramics industry, the choice of pigments used for colouring or surface treating has become vital to improving the quality of products. In order to have a wide variety of colours, the manufacturer in this area is always looking for new stable colours while optimising manufacturing costs. Mixtures of certain oxides, such as CoO, ZnO, Al₂O₃ and Cr₂O₃, are traditionally the most used pigments. Various shades of colours can be obtained, in stoichiometric quantities, from these reagents calcined at high temperatures [1–6]. Quite recently, considerable attention has been paid to inorganic pigments of oxides with the formula AB₂O₄, in which A²⁺ are accommodated in tetrahedral positions, whereas B³⁺ are in octahedral positions. This material is a double oxide of a spinel-type structure with cubic symmetry and a space group of Fd-3m, and it has very important mechanical and optical properties. The substitution of chromophore ions (mainly transition metals) within these oxides makes it possible to obtain a wide variety of colours [7–15]. Zhang et al. [16] prepared the spinel solutions Mg_{1-x}Zn_xAl_{1.8}Cr_{0.2}O₄ and studied the relationship between cation distribution and optical absorption performance in order to explain the difference in colours.

In this paper, we focused on the green ceramic pigments based on CoCr₂O₄ doped with aluminium. Previous studies have presented certain materials with shades of green colours obtained by Cr-doped Al₂O₃, ZnAl₂O₄, MgAl₂O₄ or MgAl₂Si₃O₁₂ oxides [2,17,18]. The conventional method of synthesis of these types of oxides is via solid-state reaction of mechanical mixtures of metal oxides at a high temperature. Although this process is relatively inexpensive, it generally results in inhomogeneity of the powders and poor control of the stoichiometry. Furthermore, the sintering caused by calcination at a high temperature leads to materials with a low specific surface [19]. The focus of recent research has been on chemical synthesis, in which the powders are synthesised in liquid systems. Thus, several authors have proposed different synthesis routes, such as hydrothermal processes [20], coprecipitation [21],

microemulsion [22], combustion [23–25] and sol-gel [26–28]. Amongst these methods is the polymerisable complex process using the polymeric precursor, in which the metal cations are homogeneously distributed within the polymer chain. This process has the major advantage of preparing nano-sized oxide powders with high chemical and morphological homogeneities [29,30].

In this work, cobalt chromites ($\text{CoCr}_{2-x}\text{Al}_x\text{O}_4$, $0 \leq x \leq 2$) nanoparticles were prepared by polymerisable complex process. The calcination of the precursors obtained leads to the formation of the mixed oxides at a relatively low temperature. Therefore, the Al-substituted cobalt chromites obtained yield shades of green and blue. This can be related to the electronic transitions of cobalt and chromium [31,32]. The structural, morphological and optical properties are presented and discussed.

2. Experimental

2.1. Preparation of $\text{CoCr}_{2-x}\text{Al}_x\text{O}_4$, $0 \leq x \leq 2$ nanoparticles

Nanocrystalline cobalt chromite-doped aluminium ($\text{CoCr}_{2-x}\text{Al}_x\text{O}_4$, where $0 \leq x \leq 2$) nanoparticles were prepared using analytical grade cobalt nitrate ($\text{Co}(\text{NO}_3)_2 \cdot 6\text{H}_2\text{O}$; 99.0%, Sigma Aldrich), aluminium nitrate ($\text{Al}(\text{NO}_3)_3 \cdot 9\text{H}_2\text{O}$; 99.0%, Sigma Aldrich) and chromium nitrate ($\text{Cr}(\text{NO}_3)_3 \cdot 9\text{H}_2\text{O}$; 99.0%, Sigma Aldrich) as the starting materials. The total metal ion concentration was 0.2 M, and the stoichiometric molar ratio was fixed ($\text{Co}/(\text{Cr}_{2-x}\text{Al}_x) = 1/2$). Polyacrylic acid was used in excess as the chelating agent. The pH of the mixture was maintained at 7.0 by adding a small amount of pure ammonia. Then, evaporation of the aqueous solution at 80°C led to the formation of a viscous gel. After drying at 120°C over 24h, the obtained xerogel was pre-calcined at 300°C over 12h (pyrolysis) under air to remove the organic matter. The formed precursors ($\text{Pr}_0(x)$) were heat-treated at 900°C for 5h. The

produced powders ($PR(x)$) were of different shades indicating that they were strongly affected by the substituted amount x .

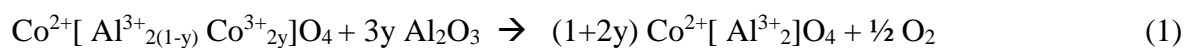
2.2. Characterization

The precursors $Pr_0(x)$ were characterised by thermogravimetric analysis (TGA) and differential thermal analysis (DTA) using a simultaneous DTA-TG apparatus (DTG-60H, Shimadzu). The heating rate was set at 2.5°C/min. The x-ray diffraction patterns were recorded with a Bruker D8 Advance x-ray diffractometer equipped with a LynxEye detector. The X-ray generator (40 kV, 40 mA) is a copper anticathode tube that uses the $CuK\alpha$ line. A graphite monochromator eliminates the $K\beta$ lines. The wavelength of the $K\alpha_1/K\alpha_2$ lines of copper is 0.15406/0.15443 nm. The phases obtained are analyzed using Eva PLUS software by comparing the positions and intensities of the different diffraction lines observed with those available in the PDF-4-2010 Database established by the ICDD (International Center for Diffraction Data). The FullProf software was used for Rietveld refinement of diagram patterns. Diffuse reflectance spectra were measured using an ultraviolet–visible spectrophotometer (Lambda 35, Perkin Elmer). The specific surface area (SSA) of the powder was measured using the Brunauer–Emmett–Teller (BET) method (Micrometrics Flowsorb II 2300 instrument). The surface morphology was examined by field emission scanning electron microscopy (JEOL JSM 6700F). The colourimetric parameters ($L^*a^* b^*$) were measured in the system Commission International de L'Eclairage (CIE) using a colourimeter (Chroma Meter CR-400/410, Konica Minolta).

3. Results and Discussion

3.1. Thermal analysis

The thermal decomposition of the precursors (Pr₀ (*x* being the aluminium amount)) was followed by thermogravimetric (TGA) and differential thermal (DTA) analyses. The temperature was gradually increased from room temperature to 1000 °C. Figs. 1 (a–c) represent TGA and DTA curves corresponding to the samples Pr₀ (*x*=0), Pr₀ (*x*=1) and Pr₀ (*x*=2), respectively. The TGA thermograms show similar thermal behaviours, with total weight losses of around 16% for the three samples analysed. These weight losses were accompanied by two DTA effects. The first (endothermic) effect is due to the elimination of water adsorbed on the surface of the powder, whereas the second (exothermic) effect is attributable to the removal of the organic residues and further crystallisation. Beyond 900°C, no discernible weight loss was observed by the TGA curves. DTA curves showed slight endothermic inflections at around 925 °C, which can be attributed to the reduction of Co³⁺ to Co²⁺. This transformation can be explained by the reaction of the mixed valence spinel structure with the amorphous alumina. According to the previous work, the equation (1) can be proposed for the composition *x*=0 [32]:



3.2. Structural analysis

In previous report based on the same spinel-type composition synthesis protocol performed on the composition *x*=0, it was shown that blue powder which represents the direct spinel was obtained from $T \geq 900^\circ\text{C}$ [32]. Therefore, in the present work, the calcination temperature was taken at 900 ° C for the synthesis of the substituted compositions. Fig.2 presents the XRD patterns of the samples heat-treated at a temperature of 900°C (PR(*x*)). The diffraction peaks of the samples with *x*=0 and *x*=2 followed the standard JCPDS card No. 080-1668 and JCPDS card No. 070-0753 for CoCr₂O₄ and CoAl₂O₄ spinels, respectively. In addition, the peaks of the Al-enriched spinels shifted towards the high angles. Therefore, the experimental values of

lattice parameter (a), determined from the XRD patterns, decreased linearly with the enrichment of Al from 8.32 Å (for $x=0$) to 8.09 Å (for $x=2$), which follows Vegard's law (Fig.3). Thus, the results were compatible with the ionic radii of Cr^{3+} ($r_{6\text{-coord}}=0.615\text{Å}$) and Al^{3+} ($r_{6\text{-coord}}=0.535\text{Å}$) in octahedral coordination, in accordance with the classification by Shannon and Prewitt [33]. It was also noted that the intensity of the (222) reflection decreased and the intensity of the (311) reflection increased with the amount of aluminium inserted (x). This finding shows that these peaks were sensitive to the nature of the atoms at the octahedral sites of the spinel structure, which can be explained by the difference in the diffusion factors of Al and Cr [34].

The Rietveld method was used to carry out structural refinements on the $\text{CoCr}_{2-x}\text{Al}_x\text{O}_4$ ($x=0, 1.0, 2.0$) samples. The corresponding data given in Table 1 show that the refined cation occupancies at the 8a sites and 16d sites confirms the spinel-type structure of the samples with a very low degree of inversion. Fig. 4a depicts the graphical illustration of the experimental, calculated and difference signals for the CoCrAlO_4 ($x=1$) sample. The Fig.4b shows the ball and stick representation of the crystal structure in which the Co^{2+} and $\text{Cr}^{3+}/\text{Al}^{3+}$ ions are located at the center of tetrahedral and octahedral O^{2-} cages, respectively. The average crystallite sizes of the samples were determined from the most intense peak (311) using Scherrer's formula [35]. As can be seen in Fig.3, the crystallite size (D) decreased with Al-enrichment from 48 nm (for $x=0$) to 22 nm (for $x=2$). This decrease almost stabilised at around 22 nm for the samples with greater than 50% Al-enrichment ($x\geq 1$).

3.3. Morphological properties

The morphologies of the powders PR (x) ($\text{CoCr}_{2-x}\text{Al}_x\text{O}_4$ where $x=0, 1.0$ and 2.0) were examined via FE-SEM analysis. The obtained micrographs are given in Fig. 5(a–c). As shown in Fig. 5a, powder PR ($x=0$) is composed of grains of variable shapes exhibiting a high state of agglomeration and an average particle size of approximately 75–200 nm. For powder PR

($x=1$), the SEM micrograph shows grains that are quasi-spherical in shape, more or less agglomerated and sized between 35 and 100 nm (Fig. 5b). Fig. 5c shows that powder PR ($x=2$) is constituted of ultrafine grains 20–40 nm in size and quasi-spherical in shape. The SSAs of the synthesised powders measured by the BET method are provided in Fig. 6. The experimental values gradually increase with aluminium substitution, from 7.4 to 12.4 m²/g for the green powders PR ($x=0$) and PR ($x=1$), respectively. For the aluminium-enriched powders ($x > 1$), the SSA continues to increase and is accompanied by a change in colour from green to blue. The particle sizes were determined from the SSAs, considering the hypothesis that the grains are spherical and mono-dispersed. These calculations were carried out using the following formula [36]:

$$d = \frac{6}{\rho \times S} 10^3 \quad (2)$$

d : particle sizes (nm).

ρ : theoretical density (cm³/g) obtained by Rietveld refinement.

S : specific surface area (m²/g).

Table 2 summarizes the results; notably, these values have the same orders of magnitude as those observed in the SEM analysis.

3.4. The colour evolution and UV-Vis analysis

The powders prepared at 900°C (CoCr_{2-x}Al_xO₄, 0 ≤ x ≤ 2) showed varying shades of blue and green colours. As shown in Fig.7, this colour shift was related to the content of the inserted Al³⁺ cations. CIE Lab colorimetric measurements and UV-Vis spectroscopy analysis were used to perform the optical characterisation of the synthesised powders.

Tristimulus colourimetry (CIELAB system) was used to measure the colour of the PR(x) powders. The ratios ($-b^*/-a^*$) and ($-a^*/-b^*$) were studied as the function of the amount (x) of aluminium inserted in order to provide a better representation of the evolution of the colour

shades. These ratios can aid in determining the dominance of blue or green colours on powders. Fig. 8 illustrates this evolution using the following three domains of the shades:

- The powders with predominantly green shades had the composition $x \leq 1$, where in the parameter $-a^*$, which was responsible for the green colour, increased and the parameter $-b^*$, which was responsible for the blue colour, was stable.
- The powders with blue-green shades had compositions corresponding to $1 < x \leq 1.4$.
- The powders with a dominant blue shade had the composition $x > 1.4$.

The UV-Vis absorption properties of the $\text{CoCr}_{2-x}\text{Al}_x\text{O}_4$ ($x=0, 1.0, 2.0$) samples were measured by diffuse reflection spectroscopy. Fig.9 shows that the spectra presented large bands in the visible region 400–950 nm. These absorptions are attributed to the spin-allowed ${}^4\text{A}_2(\text{F}) \rightarrow {}^4\text{T}_1(\text{P})$ transition of the Co^{2+} ions in the tetrahedral sites and the spin-forbidden electronic transitions ascribed to the ${}^4\text{A}_{2g} \rightarrow {}^2\text{T}_{1g}$ and ${}^4\text{A}_{2g} \rightarrow {}^2\text{E}_g$ transitions caused by the chromium (Cr^{3+}) in the octahedral site [30,37]. Using the spectra, it is possible to deduce the optical band gap energies (E_g) of the compounds. The E_g was calculated using Tauc relation [7,38]. The Kubelka-Munk (K-M) reemission function was generally applied to convert the diffused reflectance into equivalent absorption coefficient. The function K-M was given by the following equation [1]:

$$F(R) = \alpha = \frac{(1-R)^2}{2R} \quad (3)$$

where $F(R)$ is Kubulka-Munk function, α is the absorption coefficient, R is the reflectance of samples. Thus the Tauc relation becomes,

$$F(R)hv = \alpha hv = A(hv - E_g)^{n/2} \quad (4)$$

hv : energy of the incident photons (eV).

A : constant.

n : factor associated with the type of transition ($n = 1$ for a direct transition, and $n = 4$ for an indirect transition).

The energies of the forbidden bands were evaluated by considering the transition is to be direct ($n = 1$). Fig. 10 shows the variation in the plot of $(ahv)^2$ versus hv . The band gap energies (E_g) of the analysed compounds were estimated by extrapolating the linear part of the curve $(h\nu\alpha)^2$ as a function of $h\nu((h\nu\alpha)^2=0)$. The estimated values of band gap of $\text{CoCr}_{2-x}\text{Al}_x\text{O}_4$ ($x=0, 1.0, 2.0$) are 3.5, 2.68 and 2.42 eV respectively (Fig.10). These results were consistent with the results found in the literature [39–41]. The change in the band gap values would explain the colour variation of metal aluminates. Furthermore, this shift may be attributed to the difference in particle size and size distribution which can cause a variation of the optical spectra [25].

4. Conclusion

In this study, aluminium-substituted cobalt chromite nanoparticles were obtained by chemical route synthesis. The powders obtained at 900°C over 5h exhibited shades of green and blue colours. X-ray diffraction analysis showed pure phases of spinel-type structures of the $\text{CoCr}_{2-x}\text{Al}_x\text{O}_4$ ($0 \leq x \leq 2$) samples. The colorimetric measurements revealed that these solid solutions possessed three colour domains:

- $x \leq 1$, where in the green shade was dominant,
- $1 < x \leq 1.4$, where in a blue-green shade was observed,
- $x > 1.4$, wherein the compositions rich in aluminium a blue shade was dominant.

The CoCrAlO_4 ($x=1$) powder was green in colour, had quasi-spherical grains, and was more or less agglomerated. The grain size ranged between 35 and 100 nm, and the SSA was approximately 12.4 m²/g. This composition exhibited a better morphology than the green powders rich in chromium $\text{CoCr}_{2-x}\text{Al}_x\text{O}_4$ ($x < 1$).

References

- [1] W. Bao, F. Ma, Y. Zhang, X. Hao, Z. Deng, X. Zou, W. Gao, Synthesis and characterization of Fe³⁺ doped Co_{0.5}Mg_{0.5}Al₂O₄ inorganic pigments with high near-infrared reflectance, *Powder Technol.* 292 (2016) 7–13. <https://doi.org/10.1016/j.powtec.2016.01.013>.
- [2] L. Verger, O. Dargaud, M. Chassé, N. Trcera, G. Rousse, L. Cormier, Synthesis, properties and uses of chromium-based pigments from the Manufacture de Sèvres, *J. Cult. Herit.* 30 (2018) 26–33. <https://doi.org/10.1016/j.culher.2017.09.012>.
- [3] L. Verger, O. Dargaud, G. Rousse, E. Rozsályi, A. Juhin, D. Cabaret, M. Cotte, P. Glatzel, L. Cormier, Spectroscopic properties of Cr³⁺ in the spinel solid solution ZnAl_{2-x}Cr_xO₄, *Phys. Chem. Miner.* 43 (2016) 33–42. <https://doi.org/10.1007/s00269-015-0771-8>.
- [4] L. Cornu, V. Jubera, A. Demourgues, G. Salek, M. Gaudon, Luminescence properties and pigment properties of A-doped (Zn,Mg)MoO₄ triclinic oxides (with A = Co, Ni, Cu or Mn), *Ceram. Int.* 43 (2017) 13377–13387. <https://doi.org/10.1016/j.ceramint.2017.07.040>.
- [5] T. Zhang, J. Huang, J. Yan, X. Yin, Y. Wang, Pigments based on Er₂O₃-Al₂O₃: Preparation and colouring performance in zirconia ceramics, *Ceram. Int.* 46 (2020) 17523–17531. <https://doi.org/10.1016/j.ceramint.2020.04.050>.
- [6] N. Zhou, Y. Zhang, S. Nian, W. Li, J. Li, W. Cao, Z. Wu, Synthesis and characterization of Zn_{1-x}CoxO green pigments with low content cobalt oxide, *J. Alloys Compd.* 711 (2017) 406–413. <https://doi.org/10.1016/j.jallcom.2017.04.015>.
- [7] G.T. Anand, L.J. Kennedy, J.J. Vijaya, Microwave combustion synthesis, structural, optical and magnetic properties of Zn_{1-x}Co_xAl₂O₄ (0≤x≤0.5) spinel nanostructures, *J. Alloys Compd.* 581 (2013) 558–566. <https://doi.org/10.1016/j.jallcom.2013.07.081>.
- [8] L. Desouza, J. Zamian, G. Darochafilho, L. Soledade, I. Dossantos, A. Souza, T. Scheller, R. Angelica, C. Dacosta, Blue pigments based on Co_xZn_{1-x}Al₂O₄ spinels synthesized by the polymeric precursor method, *Dyes Pigments.* 81 (2009) 187–192. <https://doi.org/10.1016/j.dyepig.2008.09.017>.
- [9] A. Fernández-Osorio, C.E. Rivera, A. Vázquez-Olmos, J. Chávez, Luminescent ceramic nano-pigments based on terbium-doped zinc aluminate: Synthesis, properties and performance, *Dyes Pigments.* 119 (2015) 22–29. <https://doi.org/10.1016/j.dyepig.2015.03.021>.
- [10] M. Gaudon, L.C. Robertson, E. Lataste, M. Duttine, M. Ménétrier, A. Demourgues, Cobalt and nickel aluminate spinels: Blue and cyan pigments, *Ceram. Int.* 40 (2014) 5201–5207. <https://doi.org/10.1016/j.ceramint.2013.10.081>.
- [11] K. Kanwal, B. Ismail, K.S. Rajani, N.J.S. Kissinger, A. Zeb, Effect of Co²⁺ Ions Doping on the Structural and Optical Properties of Magnesium Aluminate, *J. Electron. Mater.* 46 (2017) 4206–4213. <https://doi.org/10.1007/s11664-017-5353-8>.
- [12] T.C. de Sousa Santos, A.C.M. Almeida, D. do Rosario Pinheiro, C.M.L. Costa, D.C. Estumano, N.F. da Paixão Ribeiro, Synthesis and characterization of colourful aluminates based on nickel and zinc, *J. Alloys Compd.* 815 (2020) 152477. <https://doi.org/10.1016/j.jallcom.2019.152477>.
- [13] S.G. Menon, K.S. Choudhari, S.A. Shivashankar, C. Santhosh, S.D. Kulkarni, Thermal effects on rapid microwave synthesized Co: ZnAl₂O₄ spinel nanoparticles, *J. Alloys Compd.* 728 (2017) 1083–1090. <https://doi.org/10.1016/j.jallcom.2017.09.085>.
- [14] J. Yan, J. Huang, T. Zhang, H. Tian, J. Yu, L. Zhang, Y. Zhang, Investigation of the microstructure, cation distribution and optical properties of nanoscale Ni_xMg_{1-x}Al₂O₄ spinel pigments, *Ceram. Int.* 45 (2019) 14073–14083. <https://doi.org/10.1016/j.ceramint.2019.04.106>.
- [15] T.C. de S. Santos, D. do R. Pinheiro, C.M.L. Costa, D.C. Estumano, N.F. da P. Ribeiro, Synthesis and characterization of pigments based on copper-zinc aluminate (Cu_xZn_{1-x}Al₂O₄) by combustion, *Ceram. Int.* 46 (2020) 2332–2343. <https://doi.org/10.1016/j.ceramint.2019.09.224>.

- [16] T. Zhang, J. Huang, J. Yan, Z. Pu, X. Yin, Y. Wang, The structural evolution and optical properties of $Mg_{1-x}Zn_xAl_{1.8}Cr_{0.2}O_4$ pink ceramic pigments, *Ceram. Int.* 45 (2019) 16848–16854. <https://doi.org/10.1016/j.ceramint.2019.05.227>.
- [17] L. Verger, O. Dargaud, N. Menguy, D. Troadec, L. Cormier, Interaction between Cr-bearing pigments and transparent glaze: A transmission electron microscopy study, *J. Non-Cryst. Solids.* 459 (2017) 184–191. <https://doi.org/10.1016/j.jnoncrsol.2017.01.016>.
- [18] M. Martos, M. Martínez, E. Cordoncillo, P. Escribano, Towards more ecological ceramic pigments: Study of the influence of glass composition on the colour stability of a pink chromium-doped ceramic pigment, *J. Eur. Ceram. Soc.* 27 (2007) 4561–4567. <https://doi.org/10.1016/j.jeurceramsoc.2007.03.030>.
- [19] S.R. Prim, A. García, R. Galindo, S. Cerro, M. Llusar, M.V. Folgueras, G. Monrós, Pink ceramic pigments based on chromium doped $M(Al_{2-x}Cr_x)O_4$, $M=Mg, Zn$, normal spinel, *Ceram. Int.* 39 (2013) 6981–6989. <https://doi.org/10.1016/j.ceramint.2013.02.035>.
- [20] Y. Chang, T. Feng, C. Wu, Y. Chen, K. Ke, Y. Liu, H. Wang, S. Dong, Controlled synthesis of blue spherical $CoAl_2O_4$ pigment powder in Pickering emulsion assisted with a hydrothermal process, *Adv. Powder Technol.* 29 (2018) 1222–1229. <https://doi.org/10.1016/j.apt.2018.02.014>
- [21] T. Ramachandran, F. Hamed, Synthesis of nanostructured pirochromite magnesium chromate with egg shell membrane template, *Appl. Nanosci.* 6 (2016) 1233–1246. <https://doi.org/10.1007/s13204-016-0538-7>.
- [22] A.E. Giannakas, A.K. Ladavos, G.S. Armatas, P.J. Pomonis, Surface properties, textural features and catalytic performance for $NO + CO$ abatement of spinels MAl_2O_4 ($M = Mg, Co$ and Zn) developed by reverse and bicontinuous microemulsion method, *Appl. Surf. Sci.* 253 (2007) 6969–6979. <https://doi.org/10.1016/j.apsusc.2007.02.031>.
- [23] J. Zhou, D. Guo, Y. Zhang, P. Rao, Combustion synthesis of $ZnFe_{2-x}Cr_xO_4$ nanocrystallites for ceramic digital decoration, *Mater. Chem. Phys.* 244 (2020) 122695. <https://doi.org/10.1016/j.matchemphys.2020.122695>.
- [24] M.A. Kassem, A.A. El-Fadl, A.M. Nashaat, H. Nakamura, Structure, optical and varying magnetic properties of insulating MCr_2O_4 ($M= Co, Zn, Mg$ and Cd) nanospinel, *J. Alloys Compd.* 790 (2019) 853–862. <https://doi.org/10.1016/j.jallcom.2019.03.189>.
- [25] T. Tatarchuk, A. Shyichuk, J. Lamkiewicz, J. Kowalik, Inversion degree, morphology and colorimetric parameters of cobalt aluminate nanopigments depending on reductant type in solution combustion synthesis, *Ceram. Int.* 46 (2020) 14674–14685. <https://doi.org/10.1016/j.ceramint.2020.02.269>.
- [26] H.R. Hedayati, A.A. Sabbagh Alvani, H. Sameie, R. Salimi, S. Moosakhani, F. Tabatabaee, A. Amiri Zarandi, Synthesis and characterization of $Co_{1-x}Zn_xCr_{2-y}Al_yO_4$ as a near-infrared reflective color tunable nano-pigment, *Dyes Pigments.* 113 (2015) 588–595. <https://doi.org/10.1016/j.dyepig.2014.09.030>.
- [27] E. Grazenaite, J. Pinkas, A. Beganskiene, A. Kareiva, Sol–gel and sonochemically derived transition metal (Co, Ni, Cu, and Zn) chromites as pigments: A comparative study, *Ceram. Int.* 42 (2016) 9402–9412. <https://doi.org/10.1016/j.ceramint.2016.02.163>.
- [28] N. Habibi, Y. Wang, H. Arandiyani, M. Rezaei, Low-temperature synthesis of mesoporous nanocrystalline magnesium aluminate ($MgAl_2O_4$) spinel with high surface area using a novel modified sol-gel method, *Adv. Powder Technol.* 28 (2017) 1249–1257. <https://doi.org/10.1016/j.apt.2017.02.012>.
- [29] Y. El Jabbar, R. El Ouatib, L. Er-Rakho, B. Durand, Influence of temperature and pH on the morphology and the color of the $CoAl_2O_4$ prepared by sol gel method, *J Mater Env. Sci.* 6 (2015) 3452–3456.
- [30] Y. El Jabbar, M. ElHafdi, M. Benchikhi, R. El Ouatib, L. Er-Rakho, A. Essadki, Photocatalytic degradation of navy blue textile dye by nanoscale cobalt aluminate prepared by polymeric

- precursor method, *Environ. Nanotechnol. Monit. Manag.* 12 (2019) 100259. <https://doi.org/10.1016/j.enmm.2019.100259>.
- [31] M. Nath, S. Song, H. Liu, Y. Li, $\text{CaAl}_2\text{Cr}_2\text{O}_7$: Formation, synthesis, and characterization of a new Cr(III) compound under air atmosphere in the $\text{Al}_2\text{O}_3\text{--CaO--Cr}_2\text{O}_3$ system, *Ceram. Int.* 45 (2019) 16476–16481. <https://doi.org/10.1016/j.ceramint.2019.05.180>.
- [32] Y. El Jabbar, H. Lakhliifi, R. El Ouatib, L. Er-Rakho, S. Guillemet-Fritsch, B. Durand, Structure, microstructure, optical and magnetic properties of cobalt aluminate nanopowders obtained by sol-gel process, *J. Non-Cryst. Solids.* 542 (2020) 120115. <https://doi.org/10.1016/j.jnoncrsol.2020.120115>
- [33] E. Finley, J. Brgoch, Deciphering the loss of persistent red luminescence in $\text{ZnGa}_2\text{O}_4\text{:Cr}^{3+}$ upon Al^{3+} substitution, *J. Mater. Chem. C.* 7 (2019) 2005–2013. <https://doi.org/10.1039/C8TC06373G>.
- [34] E. Prince, Internationale Union für Kristallographie, eds., International tables for crystallography. Vol. C: Mathematical, physical and chemical tables, 3. ed, Kluwer Acad. Publ, Dordrecht, 2004. <https://doi.org/10.1107/97809553602060000103>.
- [35] N. Hoda, F. Jamali-Sheini, Influence of synthesis parameters on the physical properties of Cu_3Se_2 nanostructures using the sonochemical method, *Ceram. Int.* 45 (2019) 16765–16775. <https://doi.org/10.1016/j.ceramint.2019.05.212>.
- [36] B. Akbari, M.P. Tavandashti, M. Zandrahimi, Particle size characterization of nanoparticles—a practical approach, *Iran. J. Mater. Sci. Eng.* 8 (2011) 48–56. [https://doi.org/10.1016/S1003-6326\(17\)60099-2](https://doi.org/10.1016/S1003-6326(17)60099-2).
- [37] Y. Gao, H. Chang, Q. Wu, H. Wang, Y. Pang, F. Liu, H. Zhu, Y. Yun, Optical properties and magnetic properties of antisite-disordered $\text{Ni}_{1-x}\text{Co}_x\text{Cr}_2\text{O}_4$ spinels, *Trans. Nonferrous Met. Soc. China.* 27 (2017) 863–867. [https://doi.org/10.1016/S1003-6326\(17\)60099-2](https://doi.org/10.1016/S1003-6326(17)60099-2).
- [38] S. Sameera, V. Vidyadharan, S. Sasidharan, K.G. Gopchandran, Nanostructured zinc aluminates: A promising material for cool roof coating, *J. Sci. Adv. Mater. Devices.* 4 (2019) 524–530. <https://doi.org/10.1016/j.jsamd.2019.10.003>.
- [39] P. Choudhary, A. Yadav, D. Varshney, Structural and optical studies of nanocrystalline ZnCr_2O_4 and CoCr_2O_4 spinel, *AIP Conf. Proc.* 1832 (2017) 050051. <https://doi.org/10.1063/1.4980284>.
- [40] L. Torkian, M. Daghighi, Effects of β -alanine on morphology and optical properties of CoAl_2O_4 nanopowders as a blue pigment, *Adv. Powder Technol.* 25 (2014) 739–744. <https://doi.org/10.1016/j.apt.2013.11.003>.
- [41] S. Rahnamaeiyan, M. Nasiri, R. Talebi, S. Khademolhoseini, Novel sol–gel method for synthesis of cobalt aluminate and its photocatalyst application, *J. Mater. Sci. Mater. Electron.* 26 (2015) 8720–8725. <https://doi.org/10.1007/s10854-015-3548-4>.

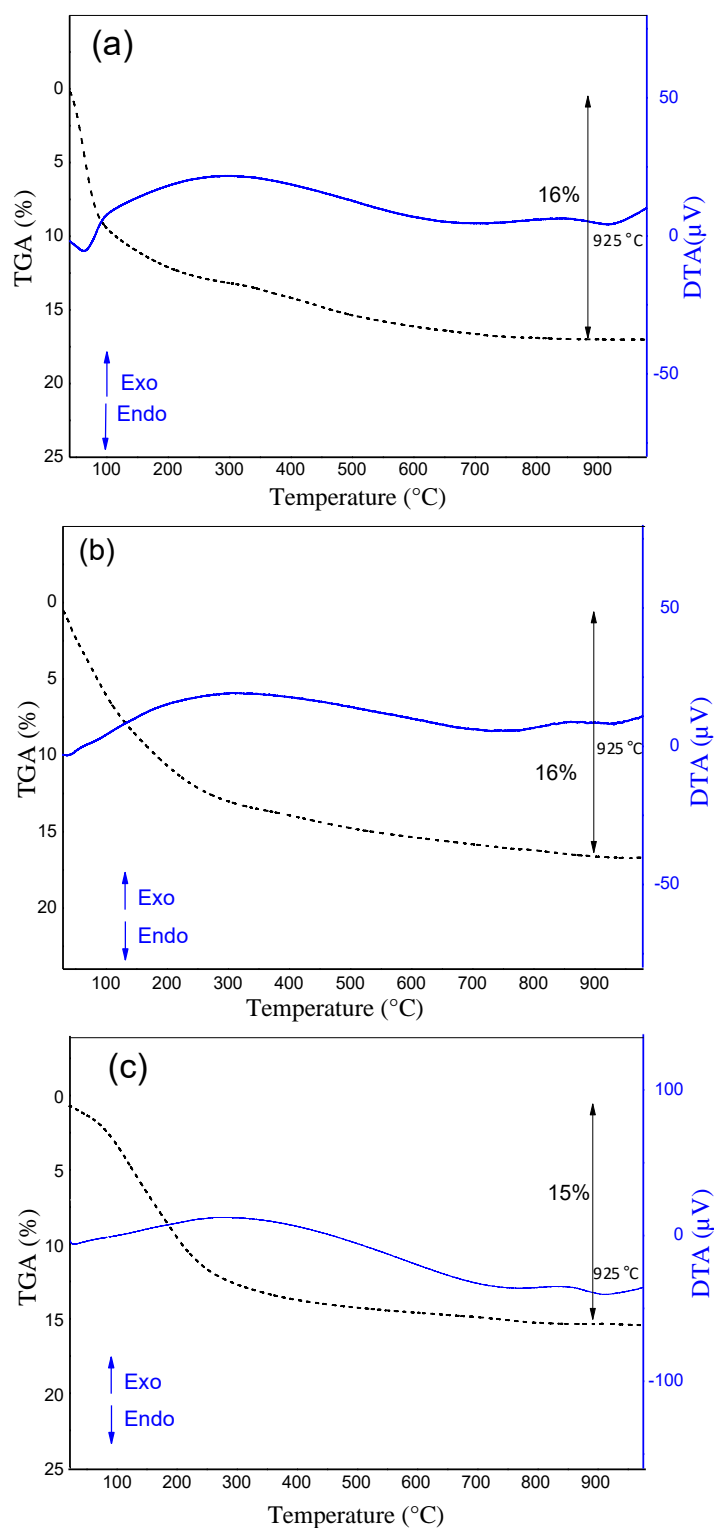


Fig.1 Thermal analysis (TGA-DTA) curves of dried gel precalcined at 300°C for 12h
Pr($x=0$) (a), Pr($x=1$) (b) and Pr($x=2$) (c).

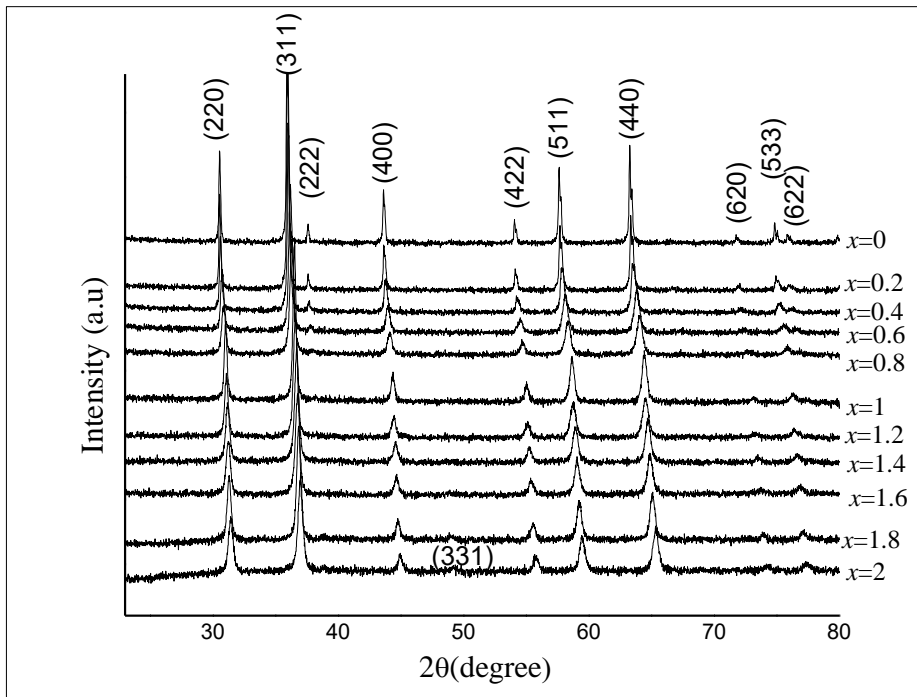


Fig.2 X-ray powder diffraction patterns of the solid solution $\text{CoCr}_{2-x}\text{Al}_x\text{O}_4$, $0 \leq x \leq 2$.

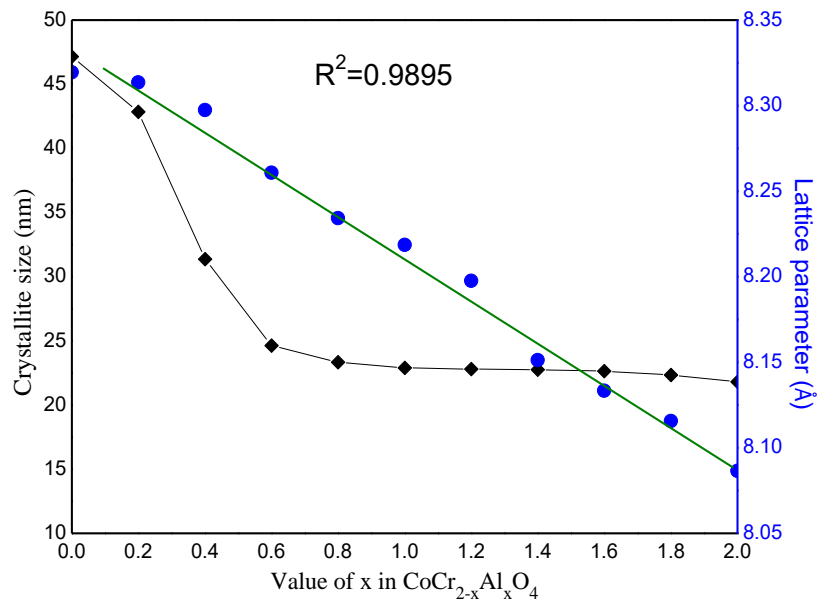


Fig.3 Lattice parameter and crystallite size of $\text{CoCr}_{2-x}\text{Al}_x\text{O}_4$ compounds as a function of the Al amount (x).

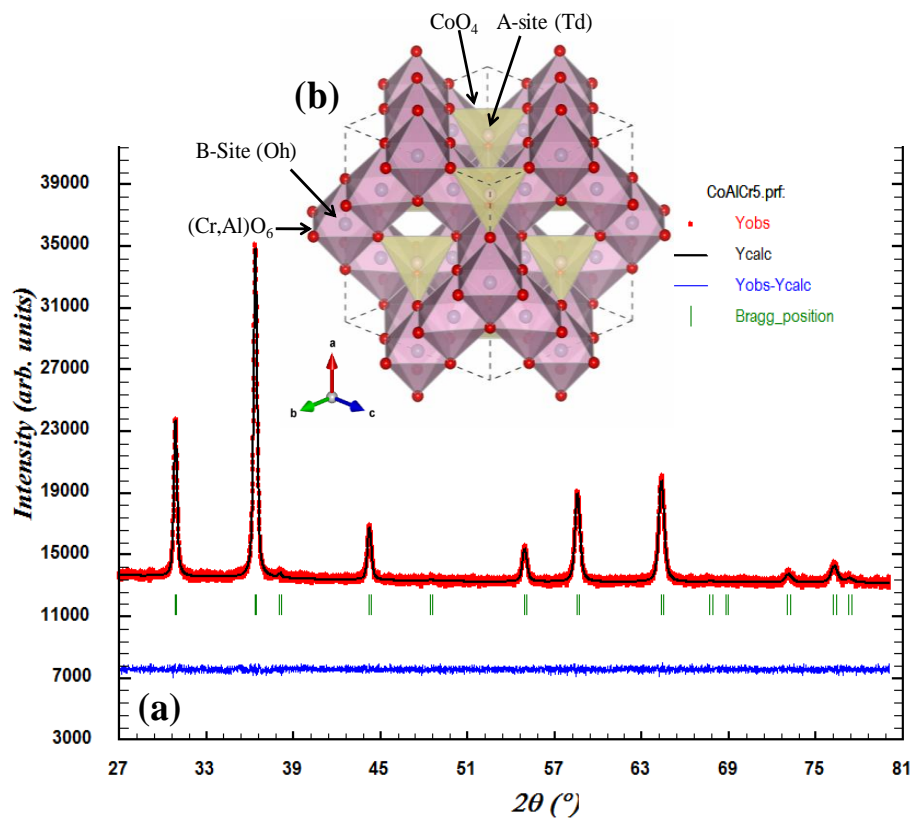


Fig.4 Rietveld refinement profiles XRD for CoCrAlO₄ sample (a), The schematic crystal structure (b).

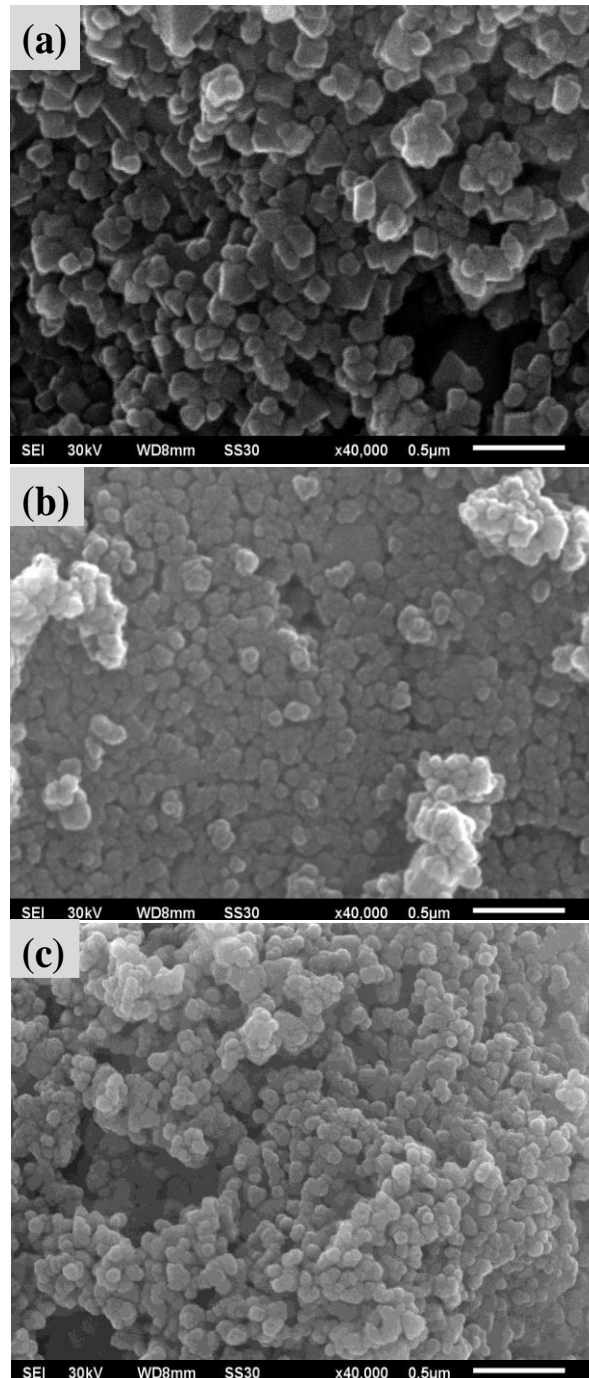


Fig.5 SEM micrographs of $\text{CoCr}_{2-x}\text{Al}_x\text{O}_4$ ($\text{PR}(x)$) powders as a function of the Al amount (x)

(a): $x=0$, (b): $x=1$ and (c): $x=2$.

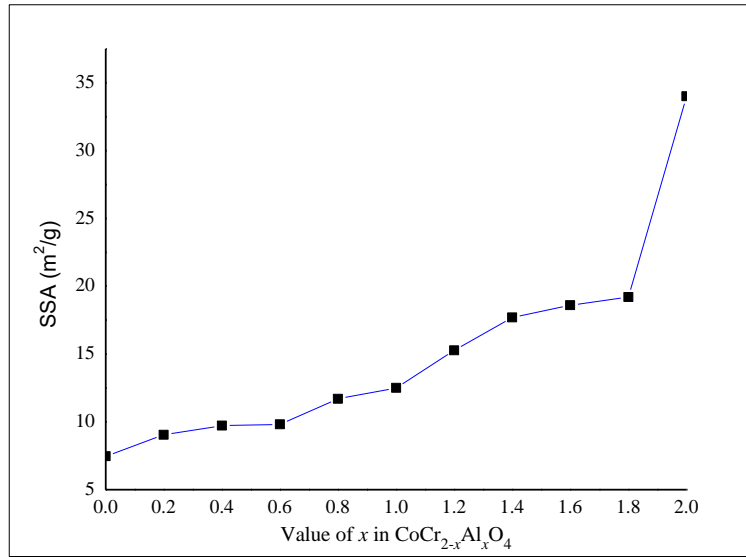


Fig.6 Surface specific area of $\text{CoCr}_{2-x}\text{Al}_x\text{O}_4$ (PR(x)) powders as a function of the Al amount (x).

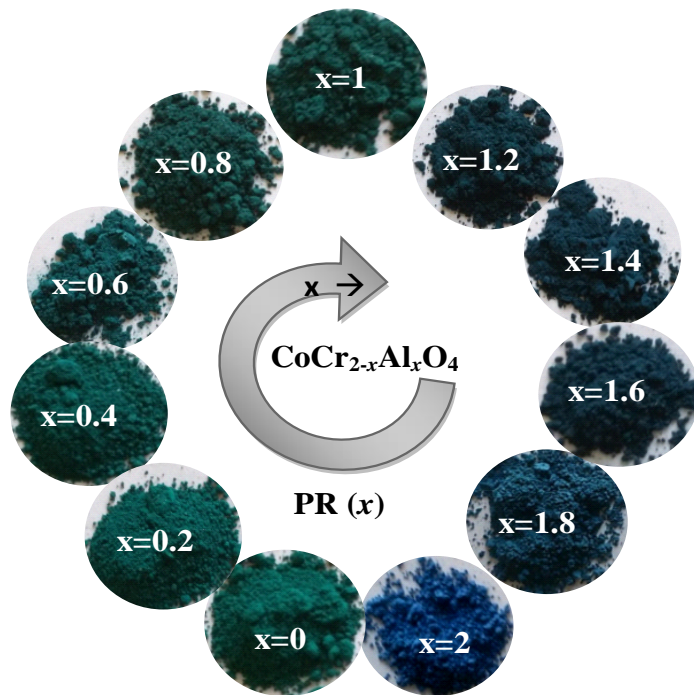


Fig.7 Powders obtained at 900°C for 5 hours (PR(x)).

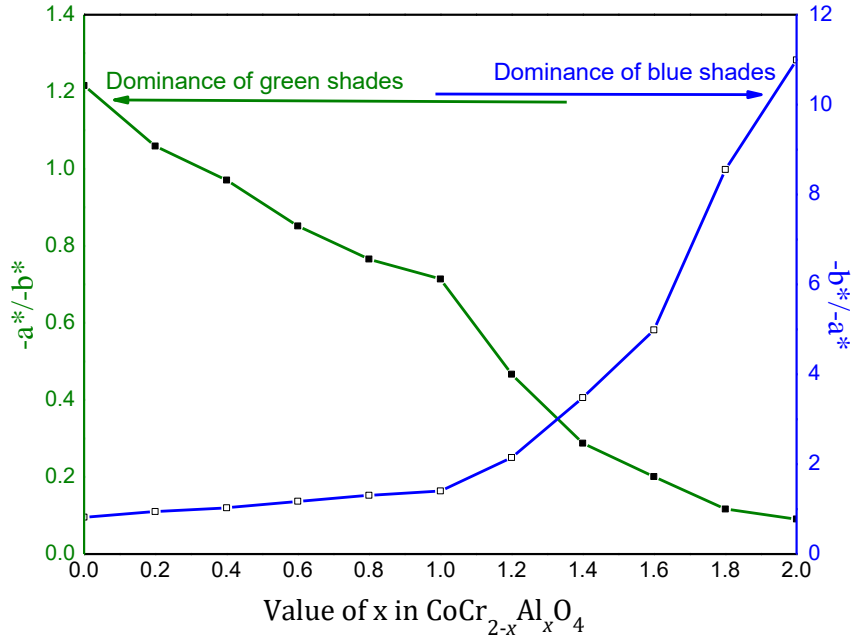


Fig.8 a^* and b^* colorimetric parameter ratios evolution of the $\text{CoCr}_{2-x}\text{Al}_x\text{O}_4$ ($0 \leq x \leq 2$) powders as a function of the Al amount (x).

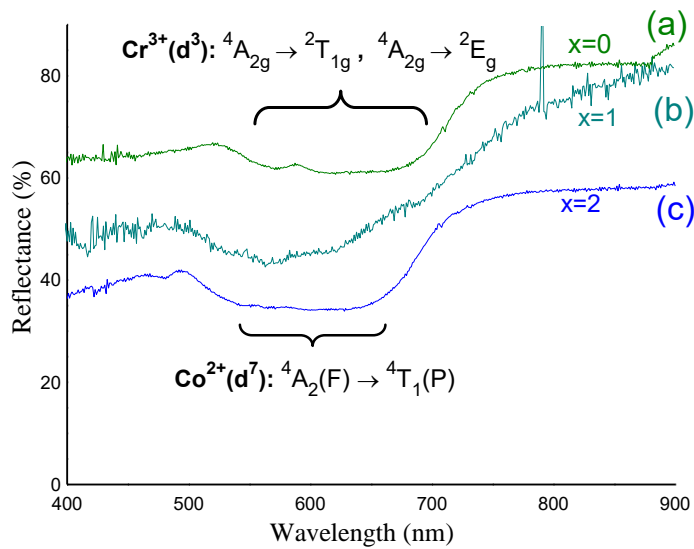


Fig.9 UV-Vis diffuse reflectance spectra of (a) CoCr_2O_4 , (b) CoCrAlO_4 and (c) CoAl_2O_4 compounds.

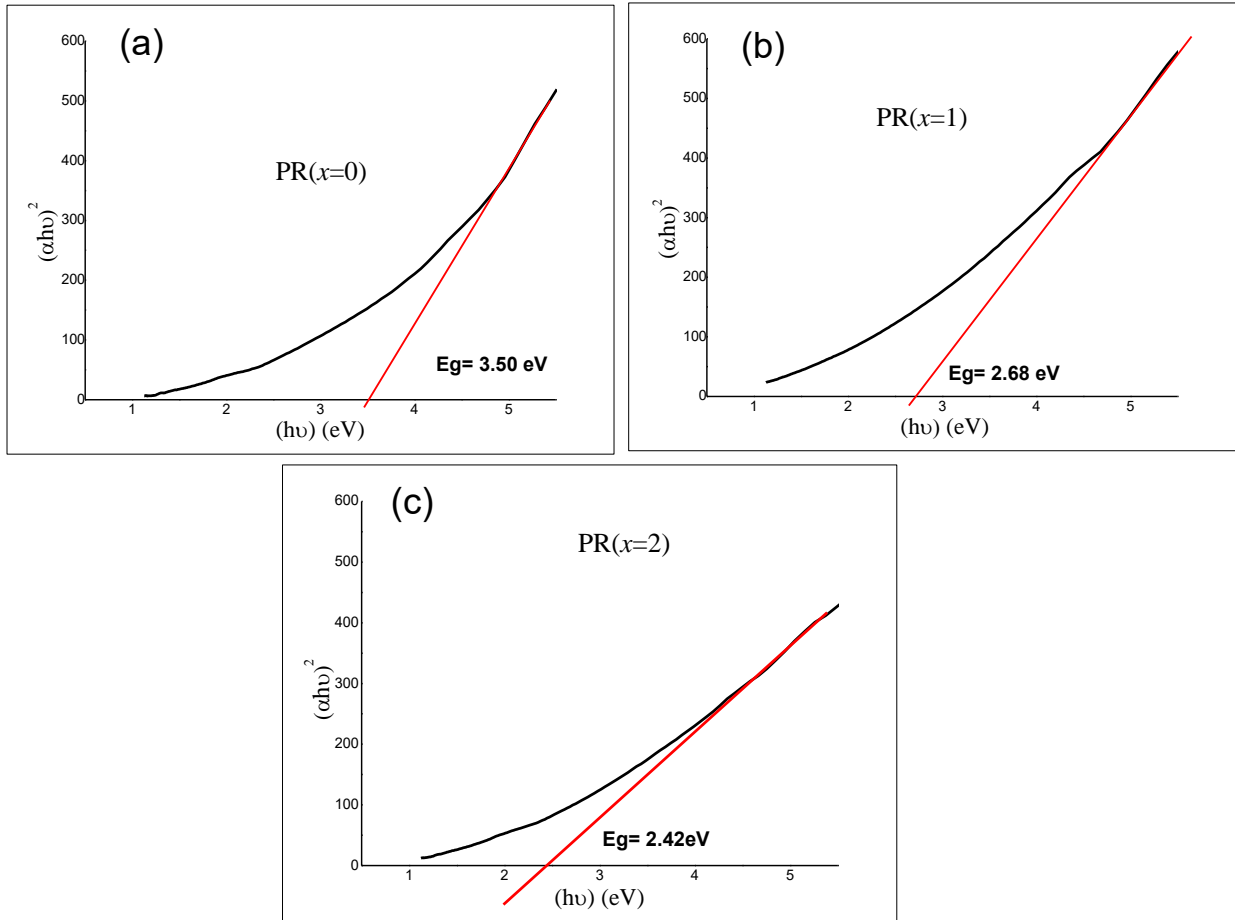


Fig.10 The plot of $(\alpha h\nu)^2$ versus $h\nu$ for (a) CoCr₂O₄, (b) CoAlCrO₄, (c) CoAl₂O₄ compounds.

Table 1Rietveld refinement for PR ($x=0$), PR ($x=1$) and PR ($x=2$) samples

Sample	Atom	Wyckoff Positions $x=y=z$	Occupancy	Biso	Refinement quality parameters
PR ($x=0$) CoCr ₂ O ₄	Co	0.125	0.97	0.727 (4)	Rp=1.35% Rwp=1.68% $\chi^2=1.10\%$
	Cr	0.125	0.03	0.727 (4)	
	Co	0.500	0.03	0.122 (3)	
	Cr	0.500	0.97	0.122 (3)	
	O	0.261(4)	1.00	0.270 (6)	
PR ($x=1$) CoCrAlO ₄	Co	0.125	0.96	0.785 (5)	Rp=0.70% Rwp=0.87% $\chi^2=1.05\%$
	Cr/Al	0.125	0.02	0.785 (5)	
	Al	0.500	0.46	0.353 (7)	
	Cr	0.500	0.44	0.353 (7)	
	Co	0.500	0.04	0.353 (7)	
	O	0.262 (3)	1.00	0.818 (5)	
PR ($x=2$) CoAl ₂ O ₄	Co	0.125	0.88	0.899 (3)	Rp=0.87% Rwp=1.08% $\chi^2=1.05\%$
	Al	0.125	0.02	0.899 (3)	
	Co	0.500	0.10	0.642 (7)	
	Al	0.500	0.84	0.642 (7)	
	O	0.263(3)	1.00	0.744 (5)	

Table 2Particle sizes and the specific surface areas of the CoCr_{2-x}Al_xO₄ ($x=0, 1.0, 2.0$) samples

Samples	Particle size range SEM (nm)	Specific surface area BET (m ² /g)	Average particle size BET (nm)
PR ($x=0$) (Green powder)	75-200	7.4	145.04
PR ($x=1$) (Green powder)	35-100	12.4	91.25
PR ($x=2$) (Blue powder)	20-40	34.26	35.72